27
570-77
25 $ NTIS

UCID- 17407

Lawrence Livermore Laboratory

PRELIMINARY THREE-DIMENSIONAL POTENTIAL FLOW SIMULATION OF A FIVE-LITER FLASK AIR INJECTION EXPERIMENT*

J. E. Davis†

March 21, 1977

*Work supported by Nuclear Regulatory Commission
†Consultant, Saratoga, California 95070

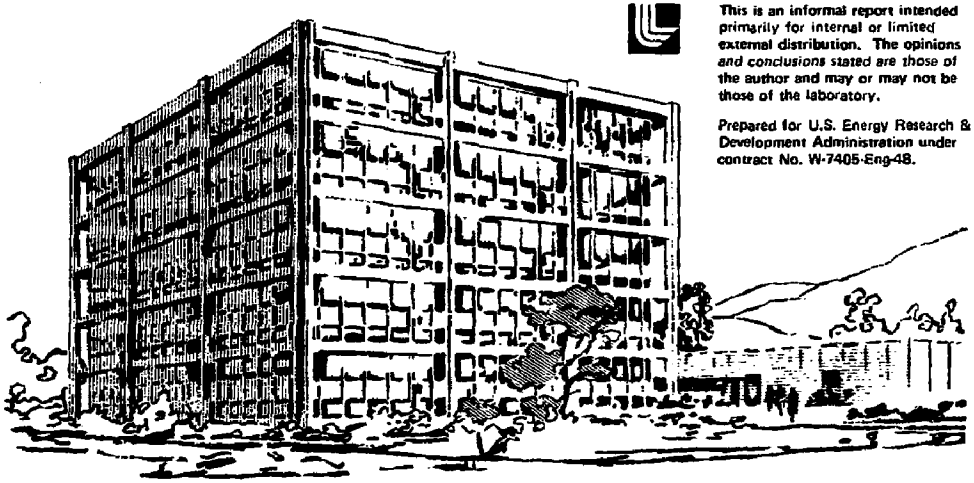

CONTENTS

PRELIMINARY THREE-DIMENSIONAL POTENTIAL FLOW SIMULATION OF A FIVE-LITER FLASK AIR INJECTION EXPERIMENTS*

ABSTRACT

The preliminary results of an unsteady three-dimensional potential flow analysis of a five-liter flask air injection experiment (small-scale model simulation of a nuclear reactor steam condensation system) are presented. The location and velocity of the free water surface in the flask as a function of time are determined during pipe venting and bubble expansion processes. The analyses were performed using an extended version of the NASA-Ames Three-Dimensional Potential Flow Analysis System (POTFAN), which uses the vortex lattice singularity method of potential flow analysis. The pressure boundary condition at the free water surface and the boundary condition along the free jet boundary near the pipe exit were ignored for the purposes of the present study. The results of the analysis indicate that large time steps can be taken without significantly reducing the accuracy of the solutions and that the assumption of inviscid flow should not have an appreciable effect on the geometry and velocity of the free water surface. In addition, the computation time required for the solutions was well within acceptable limits.

INTRODUCTION

The purpose of the present study was to obtain three-dimensional potential flow solutions simulating a five-liter flask air injection experiment and to determine the computation time required to obtain these solutions.

The five-liter flask air injection experiment is a scale model simulation of the processes that occur in the toroidal steam condensation chamber during a typical nuclear reactor cooling system operation. A schematic of the flask is shown in Fig. 1. Air is injected into the flask through the submerged pipe. The entrance of the air into the flask causes the free water surface to rise depending on the amount of air entering the flask, the rate at which it enters the flask, and the properties of the air and water. The purpose of the experiment was to determine the location and velocity of the free water surface as functions of time as a result of the air injection. This information will be used to help determine the location and velocity of the free water surface in a full-scale condensation chamber and provide a basis for predicting whether any damage to pipes or to the chamber itself could occur as a result of steam injection into the chamber.

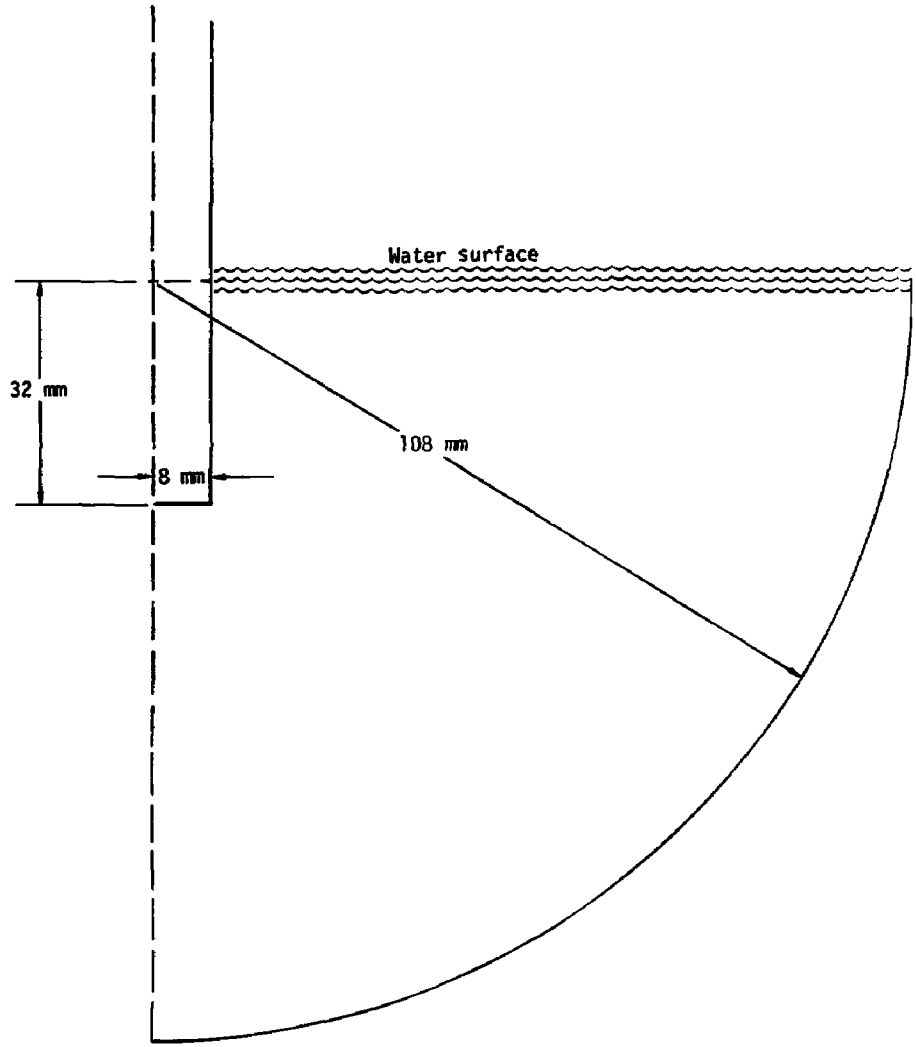

Fig. 1. Five-liter flask with submerged downcomer pipe.

The motivation for the numerical simulation of the five-liter flask experiment stems from the desire to numerically simulate the full-scale system. However, in the absence of full-scale experimental data, the experimental data from the five-liter flask experiment provides an excellent basis for comparison with the numerical results to verify the analytical assumptions.

The underlying assumption of the present analysis is that the motion of the water in the five-liter flask is both incompressible and irrotational; hence, a potential flow exists. This implies that the density of the water is constant (or the local velocity anywhere in the flask is always small compared to the speed of sound in water) and the viscous portions of the flow field are confined to regions very close to the walls or along very thin slipstreams or wakes. Analyses were performed at time intervals throughout the entire condensation process, which included pipe venting as well as bubble expansion.

A detailed description of the method of analysis is presented.

METHOD OF ANALYSIS

The unsteady three-dimensional potential flow analysis of the flow field in the five-liter flask was performed using an extension of the NASA-Ames Three-Dimensional Potential Flow Analysis System (POTFAN) which uses the vortex lattice singularity technique. A discussion of the basic unsteady potential flow assumptions and boundary conditions is given below along with a detailed description of the vortex lattice technique and the motivation for its use.

Basic Equations and Boundary Conditions

The analytical simulation of the water motion in the five-liter flask is based on the assumptions that the water is incompressible and the motion of the water is irrotational. This implies that a velocity potential, ϕ, exists throughout the flow field such that

$$\nabla^2\phi = 0 \ . \tag{1}$$

The fact that the flow is unsteady does not alter this equation, but now ϕ is a function of time as well as space, and the boundary conditions also become functions of time. The equation relating the velocity and pressure, the Bernoulli equation, now becomes

$$\frac{\partial\phi}{\partial t} + gz + \frac{v^2}{2} + \frac{P}{\rho} = \text{constant} \ , \tag{2}$$

where t = time,

g = acceleration of gravity,

z = distance of the point below the surface of the fluid,

v = magnitude of the velocity vector at the point,

p = pressure at the point,

ρ = density of the fluid.

All quantities except g and ρ are functions of time and space. The quantity z in Eq. (2) is defined at any point in the flow field by the distance from that point to the location on the current surface that is vertically above it. This quantity varies with time because the location of the free surface varies with time.

The boundary conditions to be satisfied for the current problem depend on the type of boundary. Along the wall of the flask and along the wall of the pipe, the normal component of velocity must be zero. That is,

$$\frac{\partial \phi}{\partial n} = \bar{V} \cdot \bar{n} = 0 \tag{3}$$

where $\bar{n}$ is the unit normal to the surface, and $\bar{V}$ is the velocity vector at the point. The pressure is prescribed along the surface of the water in the flask and in the pipe, and at the surface of the expanding bubble. Along the edge of the jet that issues from the pipe during venting, the normal component of velocity must be zero, the pressure must be continuous, and the location of the edge of the jet must be determined.

The Singularity Method

The equations and boundary conditions described above may be solved by any one of several potential flow techniques. The most widely used are the finite difference, finite element, and singularity techniques. Each has its own advantages and disadvantages. Since the intent of the current analytical investigation is to eventually simulate the full-scale three-dimensional process, the most appropriate technique from the standpoint of accuracy and computation time is the singularity technique. This is because the singularity technique only requires a numerical representation of the boundaries of the flow field in order to obtain a solution, whereas the other techniques require that the entire flow field be numerically represented.

The singularity technique of potential flow analysis consists of subdividing the boundary or boundaries of the flow field into quadrilateral finite elements called panels. A singularity (a function that satisfies Eq. (1) everywhere except at a point, line, or surface) is placed on each panel. An assemblage of singularities distributed over an entire boundary is referred to as the singularity distribution for that boundary. The equation that describes the velocity induced by each singularity has associated with it an influence function and a singularity strength. The product of the two defines the actual velocity induced by that singularity at any point in the flow field. The following equation expresses the velocity induced at any point in the flow field by an entire singularity distribution:

$$\bar{V}_{I1,I2} = \sum_{IS1=1}^{NS1} \sum_{IS2=1}^{NS2} s_{IS1,IS2} \hat{\bar{E}}_{IS1,IS2,I1,I2} \quad (4)$$

where $\bar{V}_{I1,I2}$ = velocity vector induced at any point in the flow field (where the point has associated with it two grid indices I1,I2) by a singularity distribution,

$\hat{\bar{E}}_{IS1,IS2,I1,I2}$ = vector velocity influence coefficient that defines the velocity induced at I1,I2 by a particular singularity (where each singularity has associated with it two grid indices IS1, IS2) whose strength is unity,

$s_{IS1,IS2}$ = the strength of the discrete singularity at IS1,IS2.

Evaluating this velocity at N locations in the flow field produces a (3 · N) matrix that may be expressed as follows:

$$\bar{V} = \hat{\bar{E}}s \quad , \quad (5)$$

where $\bar{V}$ = a (3 × N)) matrix describing the velocity vector induced at N points in the flow field by a singularity distribution,

$\hat{\bar{E}}$ = a (3 × N × M) matrix of vector velocity influence coefficients that define the velocity induced at N points in the flow field by the M discrete singularities of the singularity distribution,

s = a (1 × M) vector defining the strength of the M discrete singularities.

For a particular boundary, the strengths of the singularities may either be known or unknown depending on how the boundary condition is prescribed. For those singularities whose strengths are unknown, the boundary condition creates a system of linear algebraic equations that are solved for the unknown strengths. For those singularities whose strengths are known or are calculated from approximate analytical theories, no boundary condition need be satisfied. Instead, the velocity induced by these singularities is evaluated as a part of the known flow field. The influence of these singularities must be accounted for in satisfying the boundary conditions on other boundaries or in evaluating the velocity at arbitrary points in space. Once all the strengths have been determined, the velocity can be evaluated anywhere in the flow field or on the boundaries, and the pressure can be determined using Eq. (2).

The Finite Length Line Vortex Singularity

The type of singularity used in the present study is the finite length line vortex. It is one of the most widely used singularities in potential flow analysis by the singularity method. The reason for its broad acceptance is that the equations describing it are relatively simple. It can be used to analyze boundaries that have a net circulation (lifting or non-lifting), and since the singularity strength is a measure of the local vorticity it is a very physically meaningful quantity. References 1 through 12 provide a brief bibliography of potential flow investigations using the finite length line vortex singularity.

Since Helmholtz vortex theorems do not allow a line vortex to end in a fluid except at infinity, the vortices within a panel or from panel to panel must be linked together to form closed polygons of constant strength velocity or must extend to infinity at each end of any open polygon of linked vortices. Hence, the finite length line vortex is used in potential flow analysis problems in the form of horseshoe vortices (a finite length line vortex linked at each end to line vortices that extend to infinity), vortex quadrilaterals (four finite length line vortices linked together to form a four-sided polygon), or ring vortices (any number of finite length line vortices linked together to form a closed polygon).

The NASA-Ames Three-Dimensional Potential Flow Analysis System[2] allows for the use of all three types of finite length line vortex singularities. In the present study, the finite length line vortex is used in the form of

ring vortices linked in the circumferential direction with one finite length line vortex in each panel. Within a particular panel the line vortex lies along the front or rear edge of the panel. The location within the panel where the boundary condition is satisfied is at the centroid of the panel.

The velocity at the point (x,y,z) induced by a finite length line vortex extending from (x_1,y_1,z_1) to (x_2,y_2,z_2) is (see Fig. 2) determined by evaluating the Biot-Savart law for the special case of a vorticity distribution of constant strength Γ that is nonzero only along a straight line segment. The velocity induced by such a vorticity distribution is given by

$$(\bar{V}(x,y,z) = \frac{\Gamma(\bar{r}_1 \times \bar{r}_2)}{4\pi|\bar{r}_1 \times \bar{r}_2|^2} \bar{r}_0 \cdot \left(\frac{\bar{r}_1}{|\bar{r}_1|} - \frac{\bar{r}_2}{|\bar{r}_2|}\right) , \qquad (6)$$

where $\bar{r}_0 = (x_2 - x_1,\ y_2 - y_1,\ z_2 - z_1)$,

$\bar{r}_1 = (x - x_1,\ y - y_1,\ z - z_1)$,

$\bar{r}_2 = (x - x_2,\ y - y_2,\ z - z_2)$.

The Analytical Approximations Made for the Present Study

The boundary conditions described above are the correct ones for the current problem. However, the present version of the POTFAN computer program only possesses the capability for satisfying a specified velocity:

$$\bar{V}\cdot\bar{n} = V_{in} , \qquad (7)$$

where $\bar{V}$ = the velocity vector at a point where the boundary condition is satisfied,

$\bar{n}$ = unit vector extending from the point in any direction (not necessarily the unit normal direction),

V_{in} = specified flow through the point in the $\bar{n}$ direction.

Because the current study was intended as a demonstration of the present capabilities of the NASA-Ames Potential Flow Analysis System, it was decided to approximate or ignore the other boundary condition types for the present calculations. If the initial calculations supported the validity of the potential flow assumptions, the capability for satisfying other boundary condition types would be incorporated.

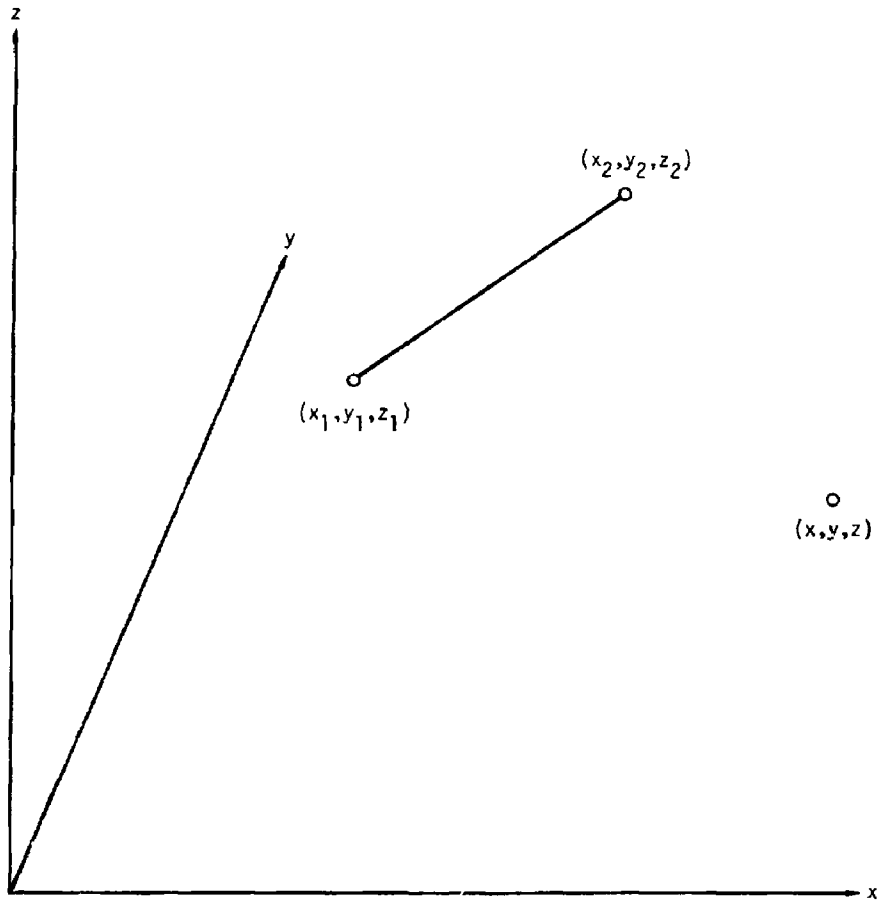

Fig. 2. The velocity induced by a finite length line vortex.

The analysis was subdivided into two separate parts. The first part consisted of the period of time during which water was ejected from the pipe into the flask. This is referred to as venting and occurs during the first 12 ms of time. During this period the walls of the flask and pipe and the free surface moving down the pipe were represented in the analysis. The second part of the analysis consisted of the duration after which all water had been ejected from the pipe. This is referred to as the bubble-expansion process and was simulated by an expanding spherical bubble centered at the bottom of the pipe. During this period the bubble and the wall of the flask were simulated, but the pipe was assumed to be nonexistent. Described below are the boundary conditions applied in these two parts of the analysis.

Solid Walls of Flask and Pipe -- The correct boundary condition ($\vec{V} \cdot \vec{n} = 0$) was satisfied only along the wetted walls of the flask and pipe. The remainder of the flask and pipe in the air space were ignored.

Free Water Surface in Flask -- The specified pressure boundary condition at this surface was ignored. This was equivalent to assuming that there was no free surface and that the water flow field existed everywhere.

Free Water Surface Inside Pipe -- The pressure boundary condition on this free surface could not be ignored since it was the driving boundary. However, since this condition could not be exactly satisfied, its effect was approximated. This free surface was assumed to be a horizontal circular disk with a downward velocity of 2.67 mm/ms specified by the experimental data given in Ref. 13. At the first time step, the position of the free surface in the pipe was assumed to be at the same level as the free surface in the flask. For succeeding time steps the free surface position was moved to the location it would have reached traveling at the specified velocity. Once the free surface reached the bottom of the pipe, the computation was halted (this was assumed to occur in 12 ms). From that time forward the presence of the pipe was ignored and only the expanding bubble (see expanding bubble boundary condition approximation) and flask wall were retained as boundaries in the flow field.

Pipe Induced Jet Boundary -- During the period of time that water was being ejected from the pipe, a free jet was present in the flow field and extended from the exit of the pipe to a point downstream of the pipe. The length of the free jet at any given time was approximately equal to the distance traveled at the jet exit velocity (2.67 mm/ms) for the time since the initiation of the

flow. Because the ejection of water from the pipe occurred for only approximately 12 ms, the maximum length of the jet was only 32 mm by the end of the venting process. As a result, the free jet did not have a sufficient length to impinge on the bottom wall of the flask to form a wall jet. Hence, for the present calculations, the jet boundary conditions of zero normal velocity and continuous pressure along the free shear layer at the edge of the jet were ignored.

Expanding Bubble Surface Boundary. The bubble-expansion portion of the analysis began after all the water in the pipe had been injected into the flask. From this time forward the pipe wall was ignored, and the flow field boundaries were assumed to consist of only the flask wall and a spherical bubble expanding with time. The center of the bubble was assumed to remain stationary at a location 32 mm below the initial free water surface (the location of the pipe exit). The expansion rate of the bubble was determined on the basis of experimental data. A plot of the assumed bubble radius as a function of time is shown in Fig. 3. The expansion rate of the bubble at any given time was the slope of the curve in Fig. 3. This expansion rate was used as the flow boundary condition on the surface of the expanding bubble.

Computation of Free Surface Location

As mentioned above, the pressure boundary condition on the free water surface inside the flask was ignored in the present calculations. Since this was equivalent to assuming that a true free surface did not exist, an "imaginary" surface was created for the purpose of computing the velocity and position of the free water surface as a function of time. This was accomplished by evaluating the velocity, from the potential flow solution, at the position in the flow field that would have been occupied by the free surface. Then, the "imaginary" surface was assumed to move with this velocity until the next time step when a new velocity was evaluated at the new position. This "imaginary" surface position at a given point in time was expressed mathematically as

$$\bar{r}_{fs}^{n+1} = \bar{r}_{fs}^{n} + \bar{V}_{fs}^{n}(t^{n+1} - t^{n}) , \tag{8}$$

where $\bar{r}_{fs}^{n+1}$ = position vector of any point on the free surface at the n+1 time step,

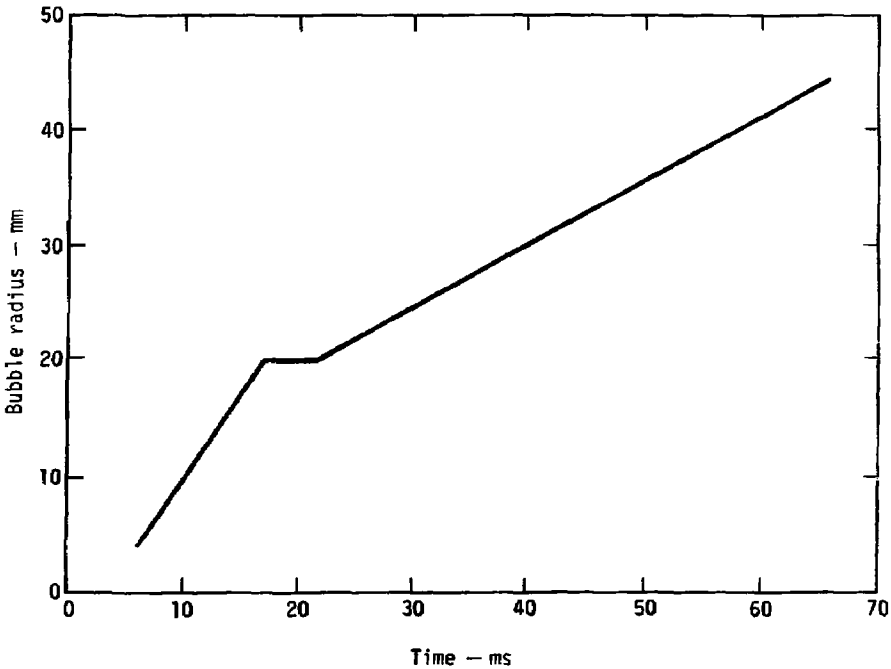

Fig. 3. Spherical bubble radius as a function of time.

$\bar{r}_{fs}^{n}$ = position vector of the same point on the free surface at the n time step,

$\bar{V}_{fs}^{n}$ = velocity vector of the point on the free surface at the n time step, and

t^{n}, t^{n+1} = the time at the n and n+1 time steps.

Because this is an entirely explicit formulation for the change in position of the free surface with time, an evaluation of the dependence of the calculation on the size of the time step was made in order to determine its accuracy. This evaluation is discussed in detail further on.

Axisymmetry Considerations

The POTFAN system of computer codes is a three-dimensional potential flow analysis tool. However, for situations where flow field symmetry exists, the system possesses special options that take advantage of the symmetry to reduce the time required to compute a solution. This is accomplished by utilizing the method of images. That is, only that part of the geometry required to uniquely define the flow field is represented to obtain the solution. The remainder of the geometry is automatically accounted for by specifying the appropriate imagery option.

Panel Size Considerations

As previously mentioned, the singularity method of potential flow analysis subdivides the boundaries of the fluid into quadrilateral panels. A potential flow singularity is placed in each panel. The accuracy of the solution generated by this technique depends to a considerable degree on the number of panels into which the boundaries are subdivided; the more panels used, the better the accuracy. However, the computation time for the solution is proportional to the cube of the number of panels. Accuracy must be sacrificed to reduce cost depending on the circumstances for each individual problem.

For the present study, a very small number of panels was used to represent the boundaries of the fluid. There were two reasons for this: 1) the current calculations were intended as a demonstration of the capabilities of the POTFAN computer program, and 2) a significant level of error already exists because some of the boundary conditions were ignored or approximated.

DISCUSSION OF RESULTS

Potential flow simulations of the five-liter flask air injection experiment were computed for several points during the entire air injection process. The computation time per time step for these solutions was 11.5 CPU seconds on a UNIVAC 1108 computer. Assuming that a CDC 7600 computer is approximately 10 times faster than a UNIVAC 1108, this value corresponds to 1.15 CPU seconds for the CDC 7600. The results are presented in the form of plots of the velocity and position of the free surface as a function of time during both the pipe venting and the bubble expansion portions of the analysis.

Pipe Venting

Potential flow simulations of the pipe-venting process were computed every 2.4 ms from t=0 to t=12 ms. The wall of the flask was represented by five panels in the azimuthal direction and 20 panels in the circumferential direction. The wall of the pipe was represented by 10 panels in the azimuthal direction and 20 panels in the circumferential direction. The free surface inside the pipe was represented by 5 panels in the radial direction and 20 panels in the circumferential direction.

Calculations of the velocity were made along the walls of the flask and pipe, along the free surface in the flask, along the centerline of the flask from the bottom of the pipe to the bottom of the flask, and radially outward from the bottom end of the pipe to the same depth at the flask wall.

An illustration of the shape of the free water surface at the beginning and end of the pipe venting process (0 and 12 ms) is shown in Fig. 4. The dashed lines in the figure refer to the locations where the velocity was computed in the interior of the flow field. As shown in the figure, most of the rise of the free water surface occurred near the center of the flask. The maximum upward velocity of the free water surface occurred during the first time step near the pipe wall and had a magnitude of about 0.08 mm/ms. This maximum velocity decreased with time until it reached 0.066 mm/ms during the last time step (12 ms). Along the flask wall the velocity reached a maximum at the free water surface but was much smaller in magnitude than near the pipe wall. During the first time step this maximum velocity on the flask wall was 0.79×10^{-3} mm/ms and at the last time step was 0.71×10^{-2} mm/ms.

From these results, estimates were made of the significance of the approximations that were made about the behavior of the flow field and its

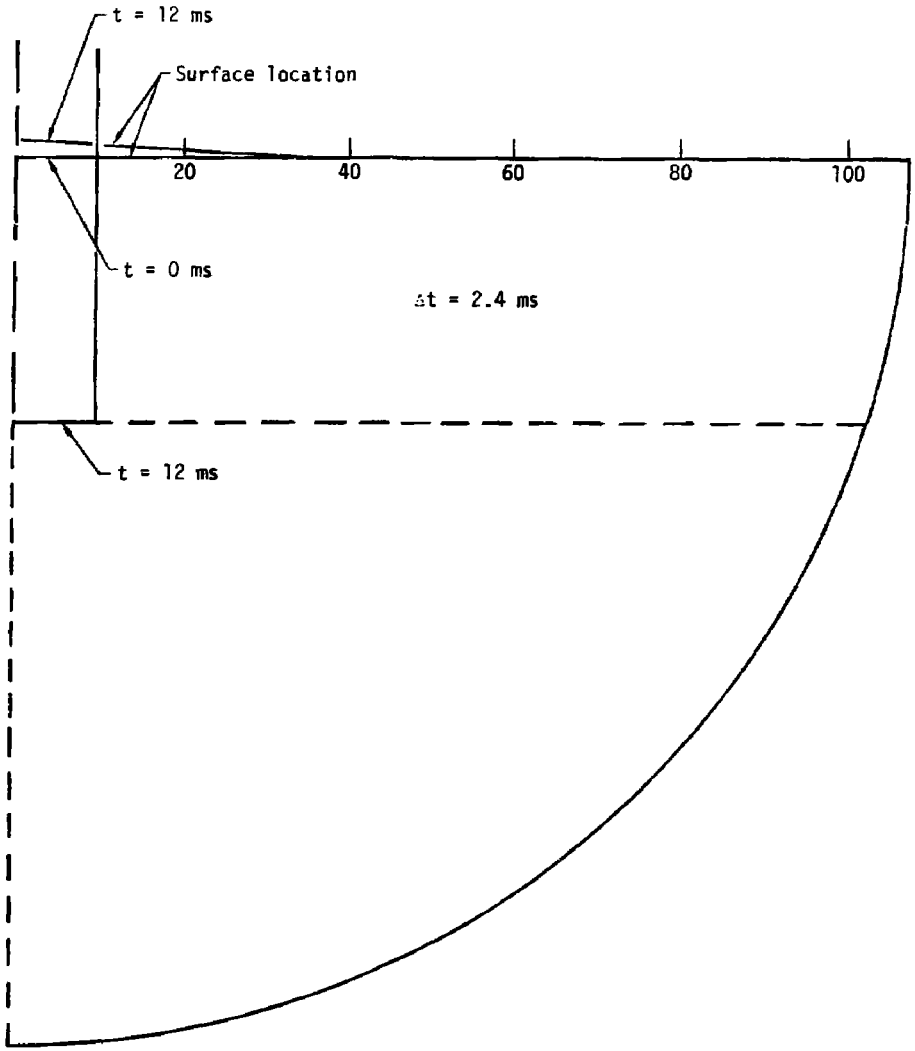

Fig. 4. Five-liter flask during pipe venting. Free surface location vs time.

boundaries. The main approximations for the pipe venting portion of the analysis were the assumptions of inviscid flow, no pressure boundary condition on the free surface, and no jet slipstream boundary downstream of the exit of the pipe.

Very crude estimates of the size of the viscous region (on the basis of local flask and pipe wall Reynolds numbers) indicated that during the early time steps nearly the entire flow field in the flask was viscous, while during the later time steps the viscous region was at most 30 to 40 mm thick near the wall of the flask and at most 4 mm thick near the pipe wall. Had the viscous effects been included in the analysis, the velocities would have been smaller near the flask wall and larger near the center of the flask. The velocities were already very small near the flask wall, so that the effect of reducing them further would not be very significant on the shape and velocity of the free surface. In fact, even if the entire velocity distribution at the free water surface were redistributed so that it was concentrated in the region within 25 mm of the pipe wall, the change in the velocities from the values obtained by the potential flow analysis would only have been about 10% at the early time steps and less for the later time steps.

The effect of the deletion of the pressure boundary at the free water surface could not be easily ascertained because it was difficult to accurately estimate the unsteady term in the equation expressing the relationship between pressure and velocity [Eq. (2)]. However, order-of-magnitude estimates indicate that this term was not negligible.

The exclusion of the jet slipstream boundary downstream of the pipe exit caused the velocity distribution along the free surface to be larger near the center of the flask than it would have been had the slipstream been included in the analysis. This was because the slipstream boundary condition forces the fluid exiting the pipe to continue further downstream before turning outward away from the axis of symmetry. This distributes the mass flux more evenly over the entire flask rather than concentrating it near the center.

Bubble Expansion

Two separate sets of potential flow simulations of the bubble expansion process were computed. The first set consisted of potential flow calculations of the flow field every 4 ms from t=6 ms to t=66 ms. The second set of calculations computed the flow field every 2 ms from t=18 ms to t=42 ms. The

intent of the second set of calculations was to determine the effect of smaller time steps on the location and velocity of the free water surface. The wall of the flask for both sets of calculations was represented by 5 panels in the azimuthal direction and 20 panels in the circumferential direction. The bubble surface for both sets of calculations was represented by 10 panels in the azimuthal direction and 20 panels in the circumferential direction.

Calculations of the velocity were made along the wall of the flask and on the free water surface. The position of the free surface at t=6 ms was assumed to be the same as at t=0 ms. However, for the 2-ms-interval calculations, the position of the free surface at t=18 ms was assumed to be the position as computed by the 4-ms-interval calculations. Illustrations of the velocity and location of the midline of the free surface as functions of time are shown in Figs. 5 and 6 for both the 2-ms- and 4-ms-interval solutions. The free water-surface and bubble-surface locations as functions of time are shown in Fig. 7. As shown in Figs. 5 and 6, there was very little difference between the 2-ms- and 4-ms-interval solutions. In fact, after 42 ms, the difference between the positions of the free surface as computed with the 2-ms- and 4-ms-intervals was only 2.33%. The close agreement between the two sets of solutions was caused by two compensating effects. The first effect of the shorter time intervals was a more accurate integration of the free surface velocity to determine its location. The location of the free surface was computed to be further away from the bubble surface than at the same time using longer time intervals. However, this produced a second effect, which nearly compensated for the first. That is, the further away the free surface was from the bubble surface, the smaller was the velocity induced at the free surface by the expanding bubble. Hence, to determine the new free surface location, the integral over the next time step would be smaller because the induced velocity was smaller during that time step. Thus, the very effect that caused the free surface to be located further from the bubble during a particular time step also caused a compensating effect that located it closer to the bubble on the next time step.

Low local Reynolds numbers along the wall of the flask caused the viscous region to engulf the majority of the flask flow field. However, the mass flux was already concentrated near the center of the flask so that any correction to

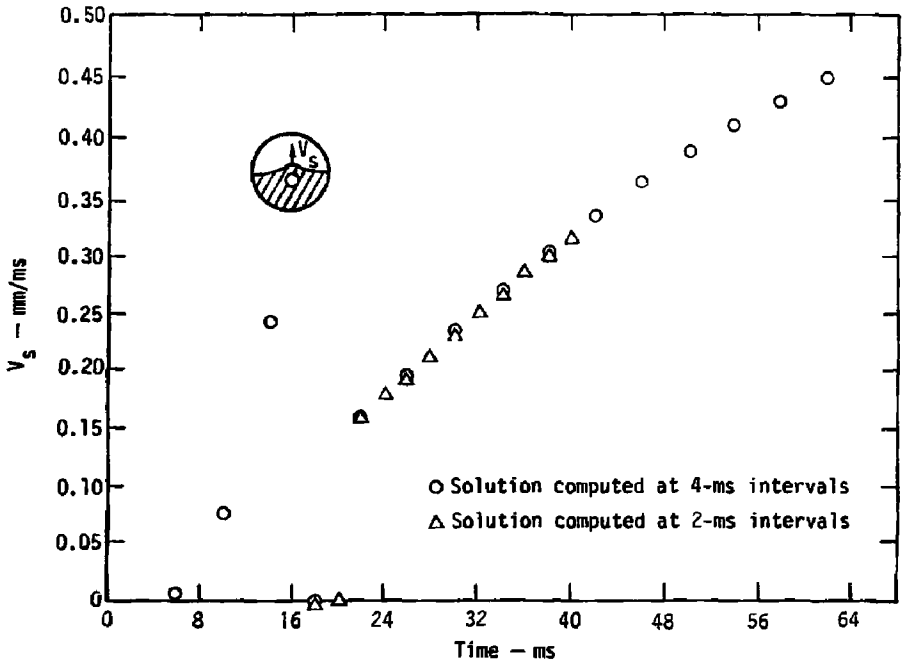

Fig. 5. Five-liter flask during bubble expansion showing centerline free surface velocity vs time.

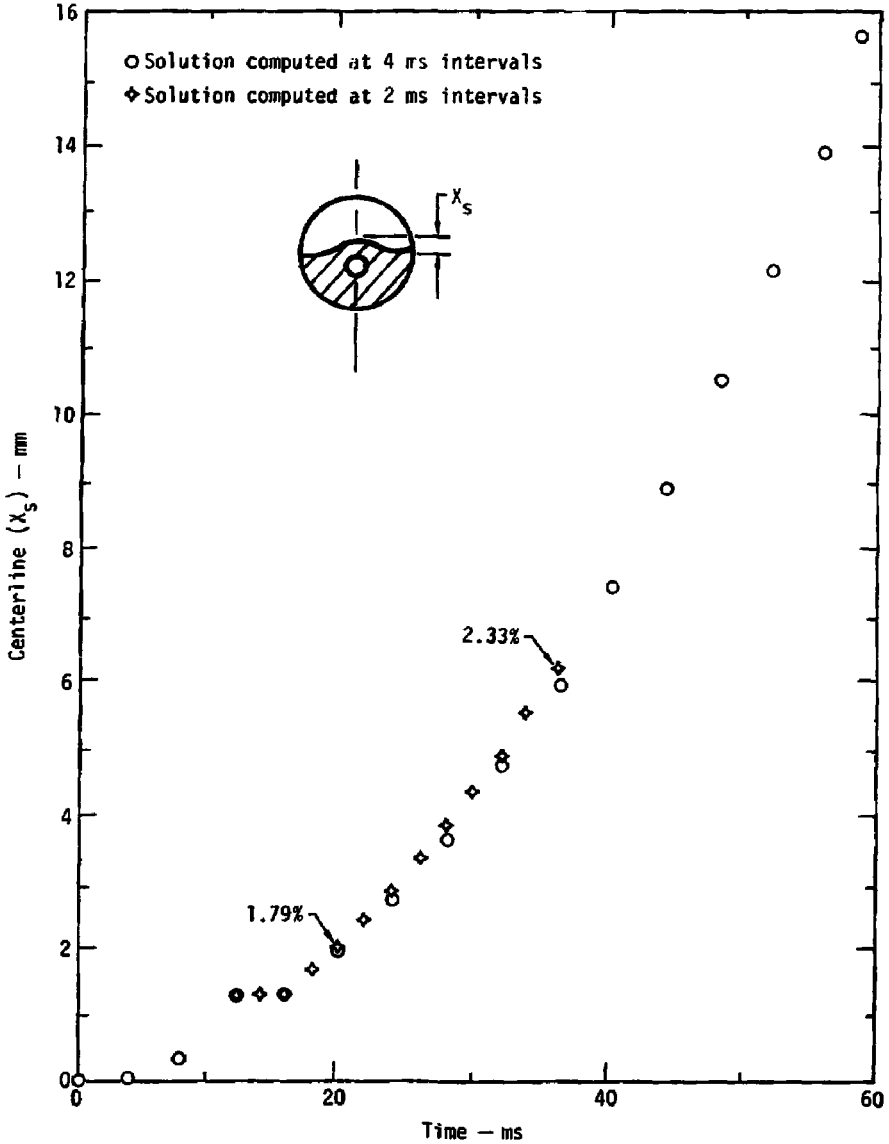

Fig. 6. Five-liter flask during bubble expansion showing the location of free surface centerline vs time.

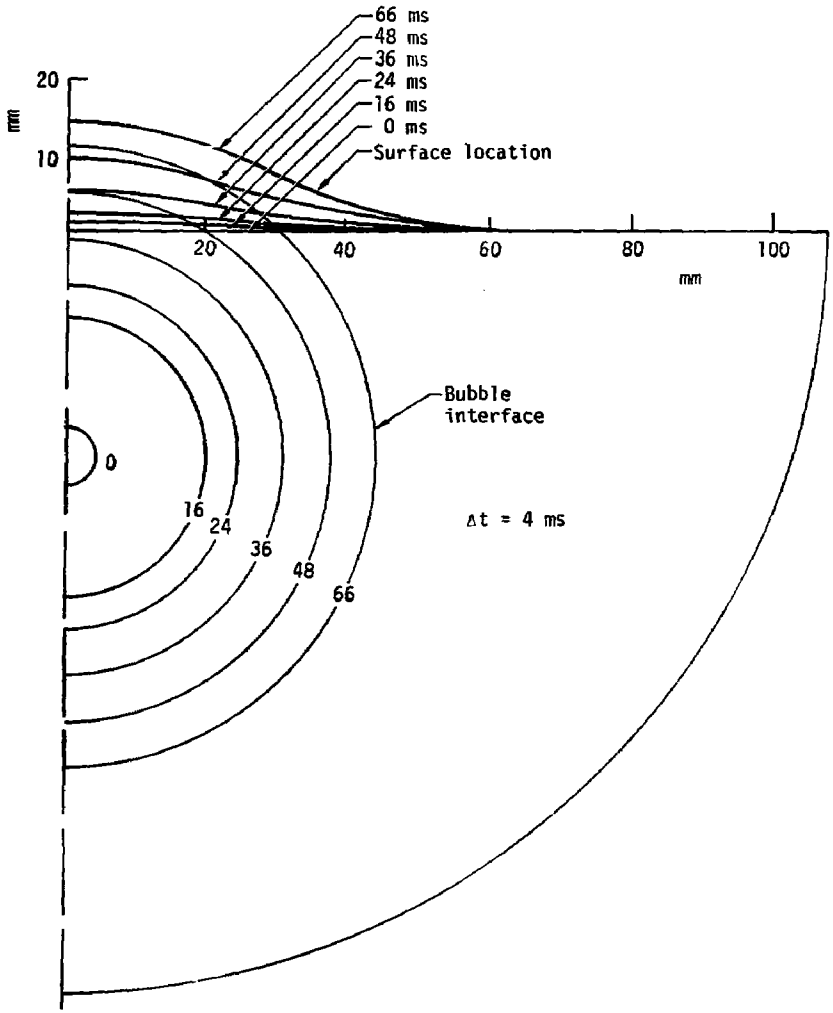

Fig. 7. Five-liter flask during bubble expansion showing bubble and free surface location vs time.

the position of the free surface and the velocity distribution along the free surface due to the inclusion of viscous effects would have been small.

The inclusion of the pressure boundary condition in the bubble expansion would have introduced two major influences on the calculation: the time-dependent term in Eq. (2) and the pressure variation in the air above the water in the flask. The present calculations did not contain sufficient information to make an accurate estimate of the time dependent term in Eq. (2). However, rough estimates indicate that this term would have contributed more than a 3% effect on Eq. (2) for the time period from 22 ms to 66 ms and an even larger effect for the period from 6 ms to 18 ms. This influence was estimated assuming that the bubble expansion process occurred as an expanding sphere. However, for a calculation where the bubble expansion process would have been represented more accurately it would have been very difficult to estimate the effect of the time-dependent term without actually performing the analysis with its influence included.

The change in pressure of the air above the water in the flask affected the analysis in a more straightforward manner. After 66 ms, the volume of the spherical bubble was about 13% of the volume originally occupied by the air in the flask above the water. A similar percentage increase in the pressure of the air above the flask would have occurred as a result of this volume displacement. This would have resulted in a 25% change in the pressure differential between the free surfaces in the flask and pipe,[13] and would have had a strong effect on the resultant flow field.

CONCLUSIONS

The results of the present study indicate that the potential flow technique is a reasonably accurate and yet inexpensive method for determining the geometry and velocity distribution of the free water surface in a numerical simulation of the five-liter flask air injection experiment. The viscous region of the flow field was found to encompass the majority of the flask. However, due to the extremely small velocities in this region, the effect of assuming an inviscid flow caused an error of about 10% in the location and velocity distribution of the free water surface. For a full-scale steam condensation process, the Reynolds numbers would be much larger so that the error in assuming an inviscid flow would be even less significant.

The exclusion of the pressure boundary conditions at the free surfaces caused significant error in the results at all time steps. The exclusion of the jet freestream boundary condition during pipe venting affected the velocity distribution at early time steps but did not strongly affect the results for later time steps.

The computation time required to obtain the solutions for the present study was very small. However, relatively few panels were used to represent the boundaries of the flow field. In a three-dimensional analysis much more computation time would be required to obtain a solution. In fact, a thousand-panel three-dimensional potential flow analysis of a full-scale steam condensation process would require a computation time per time step of between one and seven minutes on a CDC 7600.

REFERENCES

1. J. E. Davis, and L. E. Olsen, "The Constraint Function Technique Applied to the Potential Flow Analysis of Multi-Element Airfoils," NASA TM-X , 1976 (to be published).
2. R. T. Medan, "Overview of the NASA-Ames Three-Dimensional Potential Flow Analysis System (POTFAN)," 1976 (to be published).
3. B. Maskew, *A Subvortex Technique For the Close Approach to a Discretized Vortex Sheet*, NASA TM-X-62,487 (1975).
4. Tulinius, J., *Theoretical Prediction of Airplane Stability Derivatives at Subcritical Speeds*, North American Rockwell Report NA-72-803 (1972).
5. Antulio V. Gomez, *TRW Vortex-Lattice Method Subsonic Aerodynamic Analysis For Multiple-Lifting-Surfaces (M.Surface)*, TRW Report NAS 9-12330 (1972).
6. J. E. Davis, and G. L. Harris, "Nonplanar Wings in Nonplanar Ground Effect," in *J. of Aircraft*, Vol. 10, No. 5 (1973).
7. G. R. Hough, "Remarks on Vortex-Lattice Methods," in *J. of Aircraft*, Vol. 10, No. 5 (1973).
8. J. E. Davis, "Dynamic Stability of End-Plated Ram Wings in Planar Ground Effect," in *Aerospace Technology, Inc.*, Report No. 71-15 (1971).
9. J. E. Davis, "Longitudinal Stability of Tandem Planar Wings in Ground Effect," in *Aerospace Technology, Inc.*, Report No. 71-07 (1971).
10. J. P. Giesing, *Lifting Surface Theory for Wing-Fuselage Combinations*, McDonnell Douglas Corp. Report DAC 6712 (1968).
11. P. E. Rubbert, *Theoretical Characteristics of Arbitrary Wings by a Non-Planar Vortex Lattice Method*, Boeing Company Report D6-9244 (1964).
12. V. M. Falkner, *The Calculation of Aerodynamic Loading on Surfaces of Any Shape*, British Aeronautical Research Council Report R & M 1910 (1943).
13. B. R. Bowman, "Input for NRC Calculation Comparison with Experiment," Interdepartment Memorandum, Lawrence Livermore Laboratory (September 17, 1976).

BHK/gw/vt

Printed in the United States of America
Available from
National Technical Information Service
U.S. Department of Commerce
5285 Port Royal Road
Springfield, VA 22161
Price: Printed Copy $; Microfiche $3.00

Page Range	Domestic Price	Page Range	Domestic Price
001–025	$ 3.50	326–350	10.00
026–050	4.00	351–375	10.50
051–075	4.50	376–400	10.75
076–100	5.00	401–425	11.00
101–125	5.50	426–450	11.75
126–150	6.00	451–475	12.00
151–175	6.75	476–500	12.50
176–200	7.50	501–525	12.75
201–225	7.75	526–550	13.00
226–250	8.00	551–575	13.50
251–275	9.00	576–600	13.75
276–300	9.25	601–up	*
301–325	9.75		

*Add $2.50 for each additional 100 page increment from 601 to 1,000 pages; add $4.50 for each additional 100 page increment over 1,000 pages.